


















































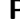






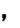


























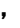










































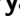
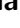












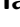






















































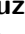




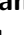

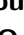








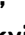





























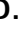



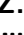



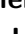





















































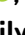






























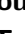
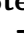

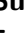












































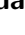

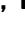

































PREPARED FOR SUBMISSION TO JHEP

Measurement of time-dependent CP violation parameters in $B^0 \rightarrow K_S^0 \pi^0 \gamma$ decays at Belle and Belle II

The Belle and Belle II Collaborations

M. Abumusabh , I. Adachi , A. Aggarwal , Y. Ahn , H. Aihara , M. Akdag , N. Akopov , S. Alghamdi , M. Alhakami , N. Alhubiti , K. Amos , M. Angelsmark , N. Anh Ky , C. Antonioli , K. Arai , H. Atmacan , V. Aushev , R. Ayad , V. Babu , H. Bae , N. K. Baghel , S. Bahinipati , P. Bambade , Sw. Banerjee , S. Bansal , M. Barrett , M. Bartl , J. Baudot , A. Beaubien , F. Becherer , J. Becker , G. F. Benfratello , J. V. Bennett , F. U. Bernlochner , V. Bertacchi , M. Bertemes , E. Bertholet , M. Bessner , S. Bettarini , V. Bhardwaj , B. Bhuyan , F. Bianchi , T. Bilka , D. Biswas , A. Bobrov , D. Bodrov , A. Bondar , G. Bonvicini , J. Borah , A. Boschetti , A. Bozek , M. Bračko , P. Branchini , N. Brenny , R. A. Briere , T. E. Browder , A. Budano , S. Bussino , F. Callet , Q. Campagna , M. Campajola , L. Cao , M. Carminati , G. Casarosa , C. Cecchi , P. Cheema , L. Chen , B. G. Cheon , C. Cheshta , H. Chetri , K. Chilikin , K. Chirapatpimol , H.-E. Cho , K. Cho , S.-J. Cho , S.-K. Choi , S. Choudhury , S. Chutia , J. Cochran , J. A. Colorado-Caicedo , I. Consigny , L. Corona , H. Crotte Ledesma , S. Cuccuini , J. X. Cui , S. Das , E. De La Cruz-Burelo , S. A. De La Motte , G. de Marino , G. De Nardo , G. De Pietro , R. de Sangro , M. Destefanis , S. Dey , R. Dhayal , A. Di Canto , J. Dingfelder , Z. Doležal , X. Dong , M. Dorigo , G. Dujany , P. Ecker , D. Epifanov , J. Eppelt , R. Farkas , P. Feichtinger , T. Ferber , T. Fillinger , C. Finck , G. Finocchiaro , F. Forti , A. Frey , B. G. Fulsom , A. Gabrielli , P. Gagneja , E. Ganiev , R. Garg , G. Gaudino , V. Gaur , V. Gautam , A. Gaz , A. Gellrich , G. Ghevondyan , D. Ghosh , H. Ghumaryan , R. Giordano , A. Giri , P. Gironella Gironell , B. Gobbo , R. Godang , O. Gogota , W. Gradl , E. Graziani , D. Greenwald , Y. Guan , K. Gudkova , I. Haide , Y. Han , K. Hayasaka , H. Hayashii , S. Hazra , C. Hearty , M. T. Hedges , A. Heidelberg , G. Heine , I. Heredia de la Cruz , T. Higuchi , M. Hoek , M. Hohmann , R. Hoppe , P. Horak , X. T. Hou , C.-L. Hsu , T. Humair , T. Iijima , K. Inami , N. Ipsita , A. Ishikawa 

R. Itoh , M. Iwasaki , P. Jackson , D. Jacobi , W. W. Jacobs , E.-J. Jang ,
Q. P. Ji , S. Jia , Y. Jin , A. Johnson , K. K. Joo , K. H. Kang , G. Karyan ,
T. Kawasaki , F. Keil , C. Kiesling , C. Kim , D. Y. Kim , H. Kim ,
J.-Y. Kim , K.-H. Kim , K. Kinoshita , P. Kodyš , T. Koga , S. Kohani ,
A. Korobov , S. Korpar , E. Kovalenko , R. Kowalewski , P. Križan ,
P. Krokovny , T. Kuhr , Y. Kulii , R. Kumar , K. Kumara , T. Kunigo ,
S. Kurokawa , A. Kuzmin , Y.-J. Kwon , S. Lacaprra , Y.-T. Lai , T. Lam ,
J. S. Lange , T. S. Lau , R. Leboucher , H. Lee , M. J. Lee , P. Leo ,
P. M. Lewis , C. Li , L. K. Li , Q. M. Li , S. X. Li , W. Z. Li , Y. Li ,
Y. B. Li , Y. P. Liao , J. Libby , J. Lin , S. Lin , Z. Liptak , V. Lisovskyi ,
C. Liu , G. Liu , M. H. Liu , Q. Y. Liu , Z. Q. Liu , D. Liventsev , S. Longo ,
A. Lozar , T. Lueck , J. L. Ma , Y. Ma , M. Maggiora , S. P. Maharana ,
R. Maiti , G. Mancinelli , R. Manfredi , E. Manoni , M. Mantovano ,
D. Marcantonio , M. Marfoli , C. Marinas , A. Martens , T. Martinov ,
L. Massaccesi , M. Masuda , T. Matsuda , D. Matvienko , S. K. Maurya ,
M. Maushart , J. A. McKenna , Z. Mediankin Gruberová , R. Mehta , F. Meier ,
D. Meleshko , M. Merola , C. Miller , M. Mirra , K. Miyabayashi , H. Miyake ,
R. Mizuk , G. B. Mohanty , S. Moneta , A. L. Moreira de Carvalho ,
H.-G. Moser , N. Mudgal , Th. Muller , H. Murakami , R. Mussa , M. Nakao ,
Y. Nakazawa , Z. Natkaniec , A. Natchii , M. Neu , S. Nishida , R. Nomaru ,
S. Ogawa , R. Okubo , H. Ono , Y. Onuki , G. Pakhlova , S. Pardi , J. Park ,
K. Park , S.-H. Park , A. Passeri , S. Patra , T. K. Pedlar , M. Piccolo ,
L. E. Piilonen , P. L. M. Podesta-Lerma , T. Podobnik , L. Polat , A. Prakash ,
V. Prasad , C. Praz , S. Prell , E. Prencipe , M. T. Prim , S. Privalov ,
I. Prudiiiev , H. Purwar , P. Rados , S. Raiz , K. Ravindran , J. U. Rehman ,
M. Reif , S. Reiter , L. Reuter , D. Ricalde Herrmann , I. Ripp-Baudot ,
G. Rizzo , S. H. Robertson , J. M. Roney , A. Rostomyan , N. Rout ,
G. Russo , S. Saha , L. Salutari , D. A. Sanders , S. Sandilya , L. Santelj ,
C. Santos , V. Savinov , B. Scavino , C. Schmitt , J. Schmitz , G. Schnell ,
K. Schoenning , C. Schwanda , Y. Seino , K. Senyo , J. Serrano , C. Sfienti ,
W. Shan , C. P. Shen , X. D. Shi , T. Shillington , T. Shimasaki , J.-G. Shiu ,
D. Shtol , B. Shwartz , A. Sibidanov , F. Simon , J. B. Singh , J. Skorupa ,
A. Soffer , A. Sokolov , E. Solovieva , S. Spataro , K. Špenko , B. Spruck ,
M. Starič , P. Stavroulakis , S. Stefkova , R. Stroili , M. Sumihama ,
M. Takahashi , M. Takizawa , U. Tamponi , K. Tanida , F. Testa , A. Thaller ,
D. V. Thanh , T. Tien Manh , O. Tittel , R. Tiwary , E. Torassa , K. Trabelsi ,
F. F. Trantou , I. Tsaklidis , M. Uchida , I. Ueda , T. Uglov , K. Unger ,
Y. Unno , K. Uno , S. Uno , Y. Ushiroda , R. van Tonder , K. E. Varvell ,
M. Veronesi , A. Vinokurova , V. S. Vismaya , L. Vitale , V. Vobbilisetti ,
R. Volpe , M. Wakai , S. Wallner , M.-Z. Wang , A. Warburton ,
M. Watanabe , S. Watanuki , C. Wessel , X. P. Xu , B. D. Yabsley ,
S. Yamada , W. Yan , W. P. Yan , J. Yelton , K. Yi , J. H. Yin ,
K. Yoshihara , C. Z. Yuan , J. Yuan , L. Yuan , Y. Yusa , L. Zani , F. Zeng 

M. Zeyrek , B. Zhang , X. Zhao , V. Zhilich , Q. D. Zhou , X. Y. Zhou ,
L. Zhu , R. Žlebčák 

ABSTRACT: We perform a measurement of time-dependent CP violation parameters in $B^0 \rightarrow K_S^0 \pi^0 \gamma$ decays using a dataset of approximately 772×10^6 and 521×10^6 $\mathcal{T}(4S)$ decays collected by the Belle and Belle II experiments, respectively. The measured parameters for the combined dataset in the $K^{*0}(892)$ dominated region ($M_{K_S^0 \pi^0} \in [0.8, 1.0] \text{ GeV}/c^2$) are $S = 0.09 \pm 0.16 \pm 0.02$ and $C = -0.09 \pm 0.08 \pm 0.04$. For the non- $K^{*0}(892)$ region ($M_{K_S^0 \pi^0} \in (1.0, 1.8] \text{ GeV}/c^2$), the corresponding values are $S = -0.32 \pm 0.33 \pm 0.09$ and $C = -0.07 \pm 0.17 \pm 0.08$. The first quoted uncertainties are statistical, while the second ones are systematic. These results are consistent with Standard Model predictions and more precise than previous measurements.

Contents

1	Introduction	1
2	Detectors and data samples	2
3	Reconstruction and event selection	4
4	Likelihood fit and results	6
4.1	Signal extraction PDF	7
4.2	CP asymmetry PDF	8
4.3	Full fit	10
4.4	Systematic uncertainties	11
5	Summary	13

1 Introduction

The study of time-dependent CP violation in the radiative decay $B \rightarrow K_S^0 \pi^0 \gamma$ provides a unique probe for physics beyond the Standard Model (SM). The decay occurs predominantly through $b \rightarrow s \gamma$ loop transitions, which makes it susceptible to contributions from heavy, virtual particles [1, 2]. As a result, this decay channel can explore physics at energy scales significantly larger than those directly accessible in current collider experiments.

The time-dependent CP asymmetry arises due to interference between decay amplitudes with and without B^0 - \bar{B}^0 mixing, where a nonzero phase appearing in the quark-mixing matrix causes differing decay rates for B^0 and \bar{B}^0 over time. For coherent $B\bar{B}$ pair production at the $\Upsilon(4S)$, in which one of the B mesons (B_{sig}) decays to a final state $f_{CP}\gamma$, where f_{CP} is a CP eigenstate, and the other B meson (B_{tag}) decays to a flavour-specific final state, this asymmetry is given as

$$\mathcal{A}_{CP}(\Delta t) = \frac{\Gamma(B_{\text{tag}=B^0}(\Delta t) \rightarrow f_{CP}\gamma) - \Gamma(B_{\text{tag}=\bar{B}^0}(\Delta t) \rightarrow f_{CP}\gamma)}{\Gamma(B_{\text{tag}=B^0}(\Delta t) \rightarrow f_{CP}\gamma) + \Gamma(B_{\text{tag}=\bar{B}^0}(\Delta t) \rightarrow f_{CP}\gamma)}, \quad (1.1)$$

where $\Gamma(B_{\text{tag}=B^0/\bar{B}^0})$ is the decay rate of B_{sig} to $f_{CP}\gamma$ when B_{tag} has been identified as a B^0/\bar{B}^0 meson, and Δt is the proper time difference between the decays of B_{sig} and B_{tag} . This asymmetry can be parameterised as

$$\mathcal{A}_{CP}(\Delta t) = S \sin(\Delta m_d \Delta t) - C \cos(\Delta m_d \Delta t), \quad (1.2)$$

where Δm_d is the mass difference between the two B^0 mass eigenstates, and S and C are the mixing-induced and direct CP -violating parameters, respectively.

In the SM, the photon emitted in $b \rightarrow s\gamma$ processes is predominantly left-handed due to the chiral structure of the weak interaction. The presence of a polarised photon in the final state suppresses the interference, leading to small CP -violating effects. In particular, the SM predicts that S should be suppressed by a factor of m_s/m_b due to helicity suppression, with deviations expected at the level of a few percent [3]. Here, m_s (m_b) is the mass of the strange (bottom) quark. The S value is calculated to be $(-2.3 \pm 1.6)\%$ for the resonant $B^0 \rightarrow K^{*0}(892)\gamma$ channel, which can, however, be enhanced to $\mathcal{O}(10\%)$ in nonresonant $B \rightarrow K_s^0\pi^0\gamma$ decays through long-distance effects, such as charm loop contributions [4, 5]. The C value is expected to be smaller than 1% [6]; however, this estimate may not be robust due to potentially large uncertainties in predicting strong phases [3].

Any significant contribution from the right-handed photon can increase the S value beyond the previously mentioned predictions, indicating evidence for new physics, such as supersymmetry, extended Higgs sectors, or models with vector-like fermions [7–9]. Therefore, a precise measurement of the time-dependent CP asymmetry in $B \rightarrow K_s^0\pi^0\gamma$ provides a stringent test of the SM and a powerful probe for new sources of CP violation from physics beyond the SM. Moreover, the different mechanisms at play in the theoretical predictions [3–5] for the $B^0 \rightarrow K^{*0}(892)\gamma$ and nonresonant decays motivate separate investigation of these channels.

The previous measurements from Belle, BaBar, and Belle II are summarised in Table 1. While these results are consistent with SM predictions, they exhibit significant uncertainties. The objective of our study is to enhance the measurement precision by utilizing a larger dataset and advanced algorithms. In particular, we have implemented an improved, Graph Neural Network (GNN)-based flavour Tagger [10] across both the Belle and Belle II datasets, along with an improved K_s^0 selection algorithm specifically for the Belle dataset. We have also incorporated information from events with poor time resolution in a time-integrated fit, which contributes to reducing the uncertainty on C .

Table 1: Summary of earlier measurements of S and C for the $B^0 \rightarrow K^{*0}(892)\gamma$ and $B^0 \rightarrow K_s^0\pi^0\gamma$ channels excluding the resonant $K^{*0}(892)$ contribution. The first quoted uncertainties are statistical, while the second ones are systematic.

Channel	Experiment	$N_{\Upsilon(4S)}$	S	C
$K^{*0}(892)\gamma$	Belle [11]	535×10^6	$-0.32^{+0.36}_{-0.33} \pm 0.05$	$0.20 \pm 0.24 \pm 0.05$
	BaBar [12]	467×10^6	$-0.03 \pm 0.29 \pm 0.03$	$-0.14 \pm 0.16 \pm 0.03$
	Belle II [13]	388×10^6	$0.00^{+0.27}_{-0.26} \pm 0.03$	$0.10 \pm 0.13 \pm 0.04$
$K_s^0\pi^0\gamma$, excluding $K^{*0}(892)\gamma$	Belle [11]	535×10^6	$0.50 \pm 0.61 \pm 0.29$	$0.20 \pm 0.37 \pm 0.13$
	BaBar [12]	467×10^6	$-0.78 \pm 0.59 \pm 0.09$	$-0.36 \pm 0.33 \pm 0.04$
	Belle II [13]	388×10^6	$0.04^{+0.45}_{-0.44} \pm 0.23$	$-0.06 \pm 0.25 \pm 0.09$

2 Detectors and data samples

The Belle and Belle II detectors both have a cylindrical geometry whose symmetry (z) axis is nearly aligned with the electron beam direction at the interaction point (IP). The polar

angle θ is defined relative to the z axis.

The Belle detector [14] was located at the KEKB accelerator [15], which collided electrons and positrons with beam energies of 8.0 GeV and 3.5 GeV, respectively. It recorded data from 1999 to 2010. Belle was a large-solid-angle magnetic spectrometer composed of a silicon vertex detector (SVD), a central drift chamber (CDC), an array of aerogel threshold Cherenkov counters (ACC), a barrel-like arrangement of time-of-flight (TOF) scintillation counters, and an electromagnetic calorimeter (ECL) comprised of CsI(Tl) crystals, all located inside a superconducting solenoid coil that provided a magnetic field of 1.5 T. The SVD and CDC were used to reconstruct charged particle tracks and vertices, while the ACC and TOF, along with specific ionization (dE/dx) measurements from the CDC, were used for charged particle identification (PID) purposes, and photons were reconstructed from calorimetric clusters in the ECL. An iron flux-return yoke, placed outside the coil, was instrumented with resistive-plate chambers to detect K_L^0 mesons and muons.

The Belle II detector [16] represents a significant upgrade from Belle, and is currently operational at the SuperKEKB accelerator [17], which collides electrons and positrons with beam energies of 7.0 GeV and 4.0 GeV, respectively. Belle II features a two-layer pixel detector (PXD) that is surrounded by a four-layer SVD [18] and a 56-layer CDC. These subdetectors help reconstruct the tracks of charged particles; the SVD and CDC additionally provide dE/dx information for PID purposes. Enclosing the CDC are a time-of-propagation counter (TOP) [19] located in the central region and an aerogel-based ring-imaging Cherenkov counter (ARICH) situated in the forward region. Together, these subdetectors constitute the primary PID system. Surrounding both the TOP and ARICH is the ECL, made from the same CsI(Tl) crystals as Belle but with faster electronics, which measures energy and time for photons and electrons. Outside the ECL is a superconducting solenoid magnet that provides a magnetic field of 1.5 T, parallel to the z axis. The flux return of the magnet is equipped with resistive-plate chambers and plastic scintillator modules for the detection of muons, K_L^0 mesons, and neutrons.

The data samples used in our study were collected at the $\Upsilon(4S)$ resonance, which decays predominantly into $B\bar{B}$ pairs. The Belle dataset corresponds to an integrated luminosity of 711 fb^{-1} , containing approximately 772×10^6 $\Upsilon(4S)$ decays. Similarly, the Belle II dataset used corresponds to an integrated luminosity of 493 fb^{-1} , containing approximately 521×10^6 $\Upsilon(4S)$ decays. About 81% of the latter sample was collected with both the PXD and SVD operational, while the remaining 19% was collected with the PXD off.

The analysis strategy and fitting procedure are developed using simulated Monte Carlo (MC) samples. Data control samples and sidebands are then used to validate the procedures before examining the signal region in the data, which is accessed only after the analysis procedures have been finalized. MC simulation samples for the process $e^+e^- \rightarrow \Upsilon(4S) \rightarrow B\bar{B}$ are generated using the EVTGEN [20] package, designed for B meson decays. The $e^+e^- \rightarrow q\bar{q}$ ($q \in [u, d, s, c]$) continuum events are generated using the KKMC [21] package. Both packages are interfaced with PYTHIA6 [22] (PYTHIA8 [23]) for Belle (Belle II). The detector response is modeled with the GEANT3 [24] framework for Belle and GEANT4 [25] for Belle II. We use MC samples from generic e^+e^- collisions, i.e., combining $B^0\bar{B}^0$, B^+B^- , and $q\bar{q}$ events, as well as specific samples of $B\bar{B}$ events, where one of the B mesons decays

into a specified mode of interest, for example, the signal. The Belle II analysis software framework [26, 27] is used to process both the simulated and real data samples.

3 Reconstruction and event selection

The reconstruction of $B^0 \rightarrow K_S^0 \pi^0 \gamma$ candidates is performed with a bottom-up approach, where K_S^0 candidates are first reconstructed from tracks in the PXD (Belle II), SVD, and CDC, while π^0 and γ candidates are reconstructed from clusters in the ECL. The remaining tracks and clusters are assigned to the B_{tag} candidates.

We reconstruct K_S^0 using two oppositely charged tracks, assumed to be pions and constrained to come from a common vertex, and that their invariant mass lies within $\pm 30 \text{ MeV}/c^2$ of the known K_S^0 mass [28]. To suppress misreconstructed K_S^0 candidates, two multivariate (MVA) classifiers are used. The first one selects K_S^0 -like candidates by primarily using the kinematic properties of the K_S^0 candidate and its decay pions, together with its flight length. The second MVA is designed to reduce the contamination from $\Lambda^0 \rightarrow p^+ \pi^-$ decays by using the proton PID likelihood of each candidate decay pion, and the reconstructed Λ^0 mass, obtained by assigning the proton mass hypothesis to one of the pion candidates. In Belle, these classifiers [29] are based on a NeuroBayes Neural Network [30] package while in Belle II, LightGBM [31] is employed.

We reconstruct π^0 candidates from two photon candidates with invariant mass satisfying $m_{\gamma\gamma} \in [90, 160] \text{ MeV}/c^2$, with further constraints on their shower shape in the ECL and the opening angle between them. For Belle II, we also require the ECL cluster time for each photon candidate to be within $\pm 200 \text{ ns}$ of the beam-crossing time. A mass-constrained fit is applied to improve the momentum resolution of π^0 candidates. To reject misreconstructed π^0 candidates, separate MVA classifiers based on XGBoost [32] are employed for Belle and Belle II utilizing features related to the kinematics of the π^0 candidates and the shower shapes of their decay products. The key discriminating features are the χ^2 probability of the mass-constrained fit and the opening angle between the π^0 decay products.

Prompt photon candidates are selected from high-energy ECL clusters with energies satisfying $E^* > 1.4 \text{ GeV}$. The asterisk (*) denotes quantities calculated in the e^+e^- center-of-mass frame. To ensure the cluster shape is consistent with an electromagnetic shower, we require that the ratio E_9/E_{21} exceeds 0.9, where E_9 and E_{21} are the energies deposited in a 3×3 array of crystals and a 5×5 array excluding the four corners, respectively, centred on the crystal with the highest energy. Furthermore, for Belle II, we require the ECL cluster time for each photon candidate to be within $\pm 200 \text{ ns}$ of the beam-crossing time. To suppress backgrounds from $\pi^0 \rightarrow \gamma\gamma$ and $\eta \rightarrow \gamma\gamma$ decays, separate MVA classifiers based on XGBoost are employed for Belle and Belle II [33]. These classifiers combine the kinematic information of the prompt photon candidate with other clusters from the rest of the event to identify potential π^0 or η candidates. If such candidates are found, then the prompt photon candidate is rejected. The most discriminating features are the reconstructed π^0/η mass and the χ^2 probability of the corresponding mass-constrained fit.

The B_{sig} candidates are reconstructed by combining the selected K_S^0 , π^0 , and prompt photon candidates. A vertex fit is performed to the entire decay chain with the B_{sig}

candidates constrained to originate from the IP [34]. Two kinematic variables are used to identify B_{sig} candidates: the beam-constrained mass $M_{\text{bc}} = (1/c^2)\sqrt{s/4 - (|\vec{p}_B^*|c)^2}$ and the energy difference $\Delta E = E_B^* - \sqrt{s}/2$, where $\sqrt{s}/2$ is the beam energy, and E_B^* and \vec{p}_B^* are the energy and momentum of the reconstructed B_{sig} candidate, respectively. Owing to the presence of a high-energy photon in the final state, the ΔE distribution is asymmetric, with a long tail on the negative side arising primarily due to shower leakage in the ECL. This effect also causes a correlation between M_{bc} and ΔE [35], which can be mitigated by redefining M_{bc} as follows:

$$\begin{aligned}
E_{\text{res}} &= \sqrt{s}/2 - E_{K_S^0}^*, \\
E'_{\pi^0} &= \frac{E_{\text{res}}}{E_{\pi^0}^* + E_\gamma^*} \times E_{\pi^0}^*, \quad E'_\gamma = \frac{E_{\text{res}}}{E_{\pi^0}^* + E_\gamma^*} \times E_\gamma^*, \\
\vec{p}'_{\pi^0} &= \sqrt{(E'_{\pi^0}/c)^2 - (M_{\pi^0}c)^2} \times \frac{\vec{p}_{\pi^0}^*}{|\vec{p}_{\pi^0}^*|}, \quad \vec{p}'_\gamma = (E'_\gamma/c) \times \frac{\vec{p}_\gamma^*}{|\vec{p}_\gamma^*|}, \\
M_{\text{bc}} &= (1/c^2)\sqrt{s/4 - (|\vec{p}_{K_S^0} + \vec{p}'_{\pi^0} + \vec{p}'_\gamma|c)^2}.
\end{aligned} \tag{3.1}$$

By rescaling the π^0 and photon energies using the precisely measured kinematics of the K_S^0 and the e^+e^- collision system, we minimize the dependence of M_{bc} on the measured energies of the π^0 and photon candidates, which are prone to biases from shower leakage. This rescaling significantly reduces the correlation between M_{bc} and ΔE in the background events without affecting the signal, and improves the signal M_{bc} resolution by 3–7% depending on the dataset. Candidates are required to satisfy $M_{\text{bc}} > 5.23 \text{ GeV}/c^2$ and $-0.3 \text{ GeV} < \Delta E < 0.2 \text{ GeV}$. The invariant mass of the $K_S^0\pi^0$ system, $M_{K_S^0\pi^0}$, is required to lie within the range $[0.8, 1.8] \text{ GeV}/c^2$. The dataset is divided into two regions: $M_{K_S^0\pi^0} \in [0.8, 1.0] \text{ GeV}/c^2$, denoted as MR1, and $M_{K_S^0\pi^0} \in (1.0, 1.8] \text{ GeV}/c^2$, denoted as MR2. The $K^{*0}(892)$ resonance is the primary contributor in MR1.

We reconstruct the B_{tag} vertex using well-reconstructed tracks not associated with the B_{sig} candidate. A further constraint is applied to ensure that the vertex lies in a tube originating from the IP, along the B_{tag} flight direction calculated using the B_{sig} momentum [36]. We retain events where both B_{sig} and B_{tag} vertices are successfully reconstructed. A GNN-based flavour tagging (FT) algorithm [10] is employed to determine the flavour of B_{tag} at the time of its decay. This algorithm outputs a flavour tag q (where $q = +1$ for B^0 and -1 for \bar{B}^0) and a quality factor r that indicates the confidence level of the flavour assignment.

The data include contributions from backgrounds associated with continuum events and $B\bar{B}$ decays other than signal. To suppress the continuum background, we train MVA classifiers based on XGBoost, using event shape variables that leverage the topological differences between $q\bar{q}$ events, which exhibit a boosted jet-like topology, and $B\bar{B}$ events, characterised by a nearly isotropic distribution. Separate classifiers are trained for Belle and Belle II, as well as for MR1 and MR2, to account for differences in detector performance and background composition. The most discriminating feature in these classifiers is the angle between the thrust axes of the B_{sig} candidate and the rest of the event. The selection criteria for all MVA classifiers are determined by maximizing a figure-of-merit $N_S/\sqrt{N_S + N_B}$,

where N_S and N_B are the numbers of signal and background events, respectively, expected in the signal region that is defined by $M_{bc} > 5.27 \text{ GeV}/c^2$ and $-0.2 \text{ GeV} < \Delta E < 0.1 \text{ GeV}$. The asymmetric range for ΔE is considered to account for the shower leakage in the ECL.

The output of the continuum MVA classifier, after applying the selection criteria, is used as a variable in the final fit. This MVA output exhibits a strong peak near 1.0 for the signal, making it challenging to model. We therefore transform it using the following relation to obtain a variable that can be more readily modeled with analytical functions:

$$C' = \ln \left(\frac{C_{\text{out}} - C_{\text{out}}^{\text{min}}}{C_{\text{out}}^{\text{max}} - C_{\text{out}}} \right), \quad (3.2)$$

where C_{out} is the original MVA output, and $C_{\text{out}}^{\text{min}}$ and $C_{\text{out}}^{\text{max}}$ are the minimum and maximum values of the output, respectively.

After applying all selection criteria, 10–12% of events have multiple signal candidates, depending on the dataset. Since these ambiguities are primarily due to misreconstructed π^0 candidates, the candidate with the highest π^0 MVA output is retained in such instances; for the remaining events with multiple candidates, a candidate is arbitrarily chosen. We find that this approach selects the correctly reconstructed signal decay in events with multiple candidates approximately 75% of the time based on simulation studies.

The overall reconstruction and selection efficiency for signal events is estimated with simulated datasets. For Belle, the efficiency is approximately 19% in MR1 and 13% in MR2. For Belle II, the corresponding values are higher, around 22% in MR1 and 14% in MR2; the increase is due to improved detector performance and reconstruction algorithms.

4 Likelihood fit and results

The distribution of the proper decay time difference Δt between B_{sig} and B_{tag} encodes the CP asymmetries [Eq. (1.2)]. This variable is calculated using the formula $\Delta t = \Delta \ell / \beta \gamma c$, where $\Delta \ell$ is the distance between the two reconstructed vertices along the boost direction, and $\beta \gamma$, the Lorentz boost of the $\Upsilon(4S)$, equals 0.425 (0.284) for Belle (Belle II).

Based on the quality of Δt reconstruction, events are categorised into two groups: well- and poorly-reconstructed Δt events. For an event to be classified as well-reconstructed, both the K_S^0 decay products must register at least one hit in the SVD layers for Belle, and in either the PXD or SVD layers for Belle II, and the uncertainty in Δt must be less than 3.0 ps for both Belle and Belle II. Such events account for approximately 50% (75%) of the total events selected in the Belle (Belle II) dataset. The larger fraction in Belle II arises from the larger volume of the vertex detector (PXD and SVD) and the smaller Lorentz boost in comparison to Belle, which enhance the likelihood of the K_S^0 decaying within the vertex detector.

The well-reconstructed Δt events are used for time-dependent (TD) fits to extract both S and C parameters, while the poorly-reconstructed Δt events are used for time-integrated (TI) fits to extract only the C parameter. To extract S and C , we perform a simultaneous extended unbinned maximum-likelihood fit to the TD and TI datasets in the two B_{tag} flavours. The TD fit involves M_{bc} , ΔE , C' , and Δt , taking per-event dependence

on the Δt uncertainty ($\sigma_{\Delta t}$) and flavour-tagging quality factor r into account. The TI fit uses M_{bc} , ΔE , and C' , considering per-event dependence on r . We use the same fit strategy for the Belle and Belle II datasets in both MR1 and MR2. The fit model includes three components: signal (both correctly and partially reconstructed events with a well-reconstructed K_s^0), $B\bar{B}$, and $q\bar{q}$ backgrounds. The probability density functions (PDFs) for all components are modelled with simulated events and validated with control channels.

Based on MC simulation studies, we find M_{bc} , ΔE , and C' variables have negligible correlation with Δt , allowing us to factorise the full fit PDFs into the two parts: the signal extraction PDF and the CP asymmetry PDF. Being a function of M_{bc} , ΔE , and C' , the first PDF aims to discriminate between various components and obtain the per-event signal probability. On the other hand, the second PDF models the Δt distribution with per-event dependence on $\sigma_{\Delta t}$ and r to determine S and C . The full PDFs for TD and TI datasets are given by:

$$P_{\text{full}}^{\text{TD}}(M_{bc}, \Delta E, C', \Delta t \mid \sigma_{\Delta t}, q, r) = \sum_{i=1}^3 N_i^q(q, r) f_i^{\text{TD}} P_i^{\text{SE}}(M_{bc}, \Delta E, C') P_i^{\text{CPV}}(\Delta t \mid \sigma_{\Delta t}, q, r) \quad (4.1)$$

and

$$P_{\text{full}}^{\text{TI}}(M_{bc}, \Delta E, C' \mid q, r) = \sum_{i=1}^3 N_i^q(q, r) (1 - f_i^{\text{TD}}) P_i^{\text{SE}}(M_{bc}, \Delta E, C'). \quad (4.2)$$

Here, $i \in [1, 3]$ represents the signal, $B\bar{B}$, and $q\bar{q}$ components, respectively; $N_i^q(q, r)$ are the yields of components for the two B_{tag} flavours, expressed in terms of the direct CP -violation parameter C for signal and $B\bar{B}$ background as described later; f_i^{TD} are the fractions of events in the TD dataset, obtained from simulation and calibrated with sidebands and control channels. Lastly, P_i^{SE} are the signal extraction PDFs, and P_i^{CPV} are the CP asymmetry PDFs for the three components.

4.1 Signal extraction PDF

We model the shape in M_{bc} for correctly reconstructed signal using a Crystal Ball function [37] with a Gaussian core and a polynomial tail on one side [38], and its ΔE shape using a Johnson's function [39]. The correlation between M_{bc} and ΔE can range from 5% to 20% depending on the dataset and is modelled in the fit by parameterising the width and tail parameters of the M_{bc} PDF as functions of ΔE . The C' distribution for signal is modelled with a Johnson's function. The signal extraction PDF for signal is then the M_{bc} - ΔE PDF multiplied by the C' PDF. The parameters describing the means of the M_{bc} and ΔE functions are floated in the full fit. For the partially reconstructed signal with a well-reconstructed K_s^0 , known as self cross-feed (SCF), we use a Crystal Ball function for M_{bc} , and an asymmetric Gaussian function for ΔE and C' . The signal extraction PDF for the SCF component is the product of the individual M_{bc} , ΔE , and C' PDFs. The final signal extraction PDF for the signal component (P_1^{SE}) is the sum of the correctly reconstructed and SCF signal PDFs, weighted by their fractions expected from MC simulation.

The $B\bar{B}$ background exhibits a peaking structure in M_{bc} near the known B meson mass [28]; however, such a structure is absent in ΔE . To address the residual correlation between M_{bc} and ΔE for this background, we model its joint M_{bc} - ΔE PDF using a two-dimensional Kernel Density Estimator (KDE) [40]. The C' distribution is represented by an asymmetric Gaussian function. The signal extraction PDF for the $B\bar{B}$ background (P_2^{SE}) is then the M_{bc} - ΔE KDE PDF multiplied with the C' PDF.

We model the $q\bar{q}$ background M_{bc} shape using an ARGUS function [41], and its ΔE shape using a first-order polynomial. The C' distribution for the $q\bar{q}$ background is modelled with a Johnson's function. Due to the negligible correlation among the three fit variables, we define the signal extraction PDF for the $q\bar{q}$ background (P_3^{SE}) as the product of the individual PDFs for M_{bc} , ΔE , and C' .

The final signal extraction PDF is the sum of signal, $B\bar{B}$, and $q\bar{q}$ background signal extraction PDFs, weighted by their respective yields, which are floated in the fit:

$$P_{\text{tot}}^{\text{SE}} = \sum_{i=1}^3 N_i P_i^{\text{SE}}(M_{bc}, \Delta E, C'). \quad (4.3)$$

To validate the signal extraction fit strategy in the data, we use the $B^0 \rightarrow K^{*0}[K^+\pi^-]\gamma$ control channel, using the same fit strategy as the signal channel. This channel is chosen because of its relatively large sample and clean signature. It mimics the signal channel due to the presence of a high-energy photon in the final state. The means of the signal and $B\bar{B}$ C' PDFs, and the widths of the signal M_{bc} , ΔE , and C' PDFs are floated in both data and simulation fits of the control channel to take into account possible data-MC differences. We extract as correction factors differences in the means and ratios in the widths, which are of the order of 1–3% for the signal and around 10% for the $B\bar{B}$ background. These correction factors are then applied to the full fit in the signal channel.

The projections of signal extraction PDFs (M_{bc} , ΔE , and C') obtained from the full fit to data in the signal channel are shown in Figures 1 and 2 for Belle and Belle II, respectively.

4.2 CP asymmetry PDF

The CP asymmetry PDF for signal comes into play in the fit performed to the Δt distribution to measure S and C . The physics-motivated model for CP violation is modified to incorporate the effect of incorrect flavour assignment by the FT algorithm, and is convolved with a resolution function to account for finite detector resolution and various physical effects, such as secondary decays of charmed particles [10]:

$$P_{\text{sig}}(\Delta t, q | \sigma_{\Delta t}, r) = \frac{\exp(-|\Delta t|/\tau_B)}{4\tau_B} \{1 - q\Delta w + q\mu(1 - 2w) + [q(1 - 2w) + \mu(1 - q\Delta w)] [S \sin(\Delta m_d \Delta t) - C \cos(\Delta m_d \Delta t)]\} \otimes \mathcal{R}(\Delta t | \sigma_{\Delta t}). \quad (4.4)$$

Here, τ_B is the lifetime of B^0 and w , Δw , and μ are the three FT parameters that represent the fraction of wrong tags, the asymmetry of wrong tags, and the asymmetry of the tagging efficiency, respectively. They are determined in seven bins of r from a control channel of

self-tagged $B^0 \rightarrow J/\psi K^*$ and $B^0 \rightarrow D^{(*)-} \pi^+$ decays for Belle and Belle II, respectively [10]. The effective tagging efficiencies are $(33.6 \pm 1.2)\%$ and $(37.4 \pm 0.4)\%$ for Belle and Belle II, respectively. We use linear interpolation to model the FT parameters as a function of r and use a per-event dependence on r in the fit.

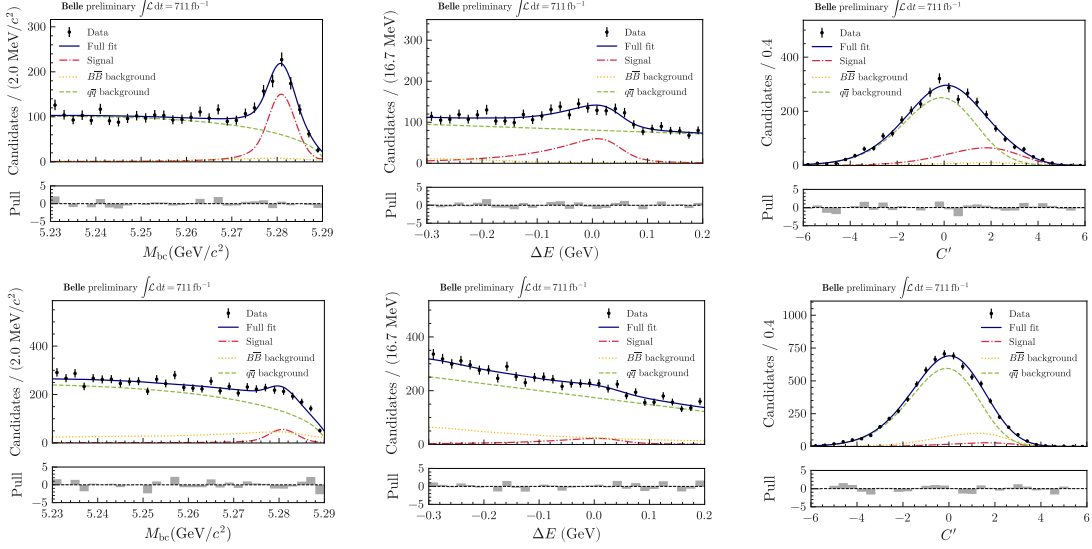


Figure 1: M_{bc} (left), ΔE (center), and C' (right) fit projections for MR1 (top) and MR2 (bottom) in Belle. Lower panels show the pulls, i.e., the differences between the data and fit results divided by the statistical uncertainty on the data.

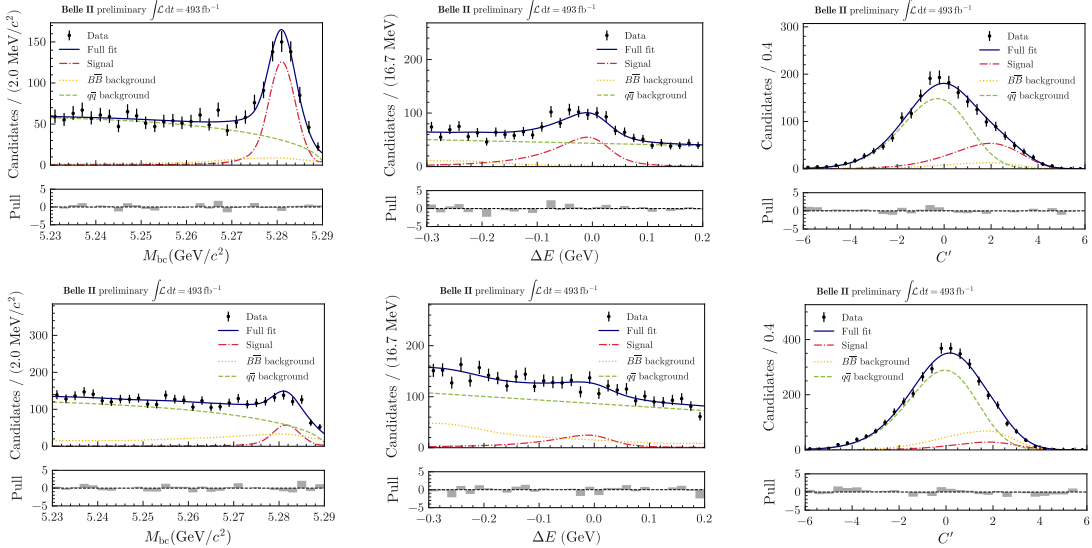


Figure 2: M_{bc} (left), ΔE (center), and C' (right) fit projections for MR1 (top) and MR2 (bottom) in Belle II. Lower panels show the pulls, i.e., the differences between the data and fit results divided by the statistical uncertainty on the data.

The resolution function $\mathcal{R}(\Delta t_{\text{res}} \equiv \Delta t - \Delta t_{\text{true}} \mid \sigma_{\Delta t})$ is modelled as the sum of a core and a tail Gaussian (G) partially convolved with an exponential function, considering per-event dependence on $\sigma_{\Delta t}$, and is given by:

$$\mathcal{R}_{\text{res}}(\Delta t_{\text{res}} \mid \sigma_{\Delta t}) = (1 - f_{\text{tail}}) \mathcal{R}_{\text{res}}^{\text{core}} + f_{\text{tail}} \left((1 - f_{\text{exp}}) \mathcal{R}_{\text{res}}^{\text{tail-G}} + f_{\text{exp}} \mathcal{R}_{\text{res}}^{\text{tail-GE}} \right), \quad (4.5)$$

$$\mathcal{R}_{\text{res}}^{\text{core}} = G(\Delta t_{\text{res}}, \mu_{\text{core}} \sigma_{\Delta t}, \sigma_{\text{core}} \sigma_{\Delta t}), \quad (4.6)$$

$$\mathcal{R}_{\text{res}}^{\text{tail-G}} = G(\Delta t_{\text{res}}, \mu_{\text{tail}} \sigma_{\Delta t}, \sigma_{\text{tail}} \sigma_{\Delta t}), \quad (4.7)$$

$$\mathcal{R}_{\text{res}}^{\text{tail-GE}} = \mathcal{R}_{\text{res}}^{\text{tail-G}} \otimes \left(f_{\text{R}} \exp\left(\frac{-\Delta t_{\text{res}}}{k \sigma_{\Delta t}}\right) + (1 - f_{\text{R}}) \exp\left(\frac{\Delta t_{\text{res}}}{k \sigma_{\Delta t}}\right) \right). \quad (4.8)$$

The parameters of the resolution functions in data and simulation are determined from fits to a control channel of $B^0 \rightarrow J/\psi K_{\text{S}}^0$ decays with the J/ψ not included in the vertexing. This channel is a good proxy for the signal channel, with the only source of vertex information coming from the K_{S}^0 decay products.

The relative signal yields in the two flavours of B_{tag} contain information about the direct CP violation parameter C . In particular, the normalisation of the signal PDF for each event in the two flavours can be expressed in terms of C as follows:

$$N_{\text{sig}}^q (q = \pm 1, r) = \frac{N_{\text{sig}}}{2} \left(1 - q \Delta w + q \mu (1 - 2w) - C \frac{q(1 - 2w) + \mu(1 - q \Delta w)}{1 + \Delta m_d^2 \tau_B^2} \right). \quad (4.9)$$

We model the $B\bar{B}$ background Δt shape using the same functional form as the signal, but with effective lifetime ($\tau_{B\bar{B}}$) and CP violation parameters ($S_{B\bar{B}}$ and $C_{B\bar{B}}$). We also use the same resolution function as that used for the signal, except for the width of the core Gaussian, which is determined from a fit to simulated $B\bar{B}$ background events. The parameter $\tau_{B\bar{B}}$ is allowed to float in the full fit. On the other hand, $S_{B\bar{B}}$ and $C_{B\bar{B}}$ are fixed to their simulation values, determined as the weighted averages of the CP violation parameters across the various background components. Furthermore, the yields of $B\bar{B}$ background in the two B_{tag} flavours are parametrised in a similar way to the signal component, but using $C_{B\bar{B}}$ instead of C . We model the Δt shape of the $q\bar{q}$ component using the signal resolution function, with the mean and width of the core Gaussian allowed to float in the final fit. The $q\bar{q}$ yield for each of the two B_{tag} flavours is half of the total continuum yield, as no CP violation is expected in this component.

The CP asymmetry fit strategy is validated using the control channel of $B^0 \rightarrow J/\psi K_{\text{S}}^0$ decays with the J/ψ removed from the vertexing, with the same fit strategy as the signal channel. The fit quality is good with the CP violation parameters measured as $S_{J/\psi K_{\text{S}}^0} = 0.65 \pm 0.06$ (0.64 ± 0.04) and $C_{J/\psi K_{\text{S}}^0} = 0.06 \pm 0.03$ (-0.04 ± 0.04) for Belle (Belle II), which are consistent with world averages [28].

4.3 Full fit

The full fit consists of a simultaneous fit to TD and TI datasets in two flavours of B_{tag} , with the respective PDFs as described above. The fit strategy is validated using large

ensembles of pseudoexperiments generated from the PDFs as well as samples drawn from MC simulation, with no significant bias observed in the fitted CP -violation parameters. Further validation is conducted by extracting the B meson lifetime [28] and CP violation parameters from the data using an ensemble of randomised flavour tags. The results are consistent with expectations.

The signal and background yields in the signal region, obtained from fits to the data, are given in Table 2. Similarly, the results for the CP violation parameters are given in Table 3. The background-subtracted [42] Δt fit projections and asymmetries, $[N_{\text{sig}}(B_{\text{tag}}^0) - N_{\text{sig}}(\bar{B}_{\text{tag}}^0)]/[N_{\text{sig}}(B_{\text{tag}}^0) + N_{\text{sig}}(\bar{B}_{\text{tag}}^0)]$, for the signal component in the TD dataset are shown in Figure 3 for the two datasets and two mass regions. The C information encoded in these projections corresponds to the TD dataset alone, which differ by up to 1.4 standard deviations from the C values obtained from the combined TD and TI datasets (Table 3).

Table 2: Signal and background yields in the signal region obtained from the fits to data. The last column shows the ratio of the signal to background yield.

Mass range	Dataset	N_{sig}	$N_{B\bar{B}}$	$N_{q\bar{q}}$	$N_{\text{sig}}/(N_{B\bar{B}} + N_{q\bar{q}})$
MR1	Belle	558 ± 29	30 ± 9	350 ± 8	1.47
	Belle II	452 ± 24	34 ± 7	178 ± 6	2.13
MR2	Belle	212 ± 26	216 ± 43	753 ± 21	0.22
	Belle II	213 ± 22	147 ± 14	350 ± 10	0.43

Table 3: CP violation parameters obtained from the full fits to data. The first uncertainties listed are statistical, and the second are systematic; the latter are discussed in Section 4.4.

Mass range	Dataset	S	C
MR1	Belle	$0.18 \pm 0.31 \pm 0.04$	$-0.01 \pm 0.12 \pm 0.04$
	Belle II	$0.04 \pm 0.19 \pm 0.02$	$-0.16 \pm 0.10 \pm 0.04$
	Belle + Belle II	$0.09 \pm 0.16 \pm 0.02$	$-0.09 \pm 0.08 \pm 0.04$
MR2	Belle	$-0.37 \pm 0.58 \pm 0.09$	$-0.01 \pm 0.29 \pm 0.07$
	Belle II	$-0.29 \pm 0.41 \pm 0.09$	$-0.11 \pm 0.22 \pm 0.09$
	Belle + Belle II	$-0.32 \pm 0.33 \pm 0.09$	$-0.07 \pm 0.17 \pm 0.08$

The results for S and C are combined across the Belle and Belle II datasets by calculating their weighted average, while accounting for correlations among the systematic uncertainties and observables [43]. The correlations between the S and C values for the Belle + Belle II dataset are approximately +5% in MR1 and -7% in MR2. The estimation of systematic uncertainties is discussed in Section 4.4.

4.4 Systematic uncertainties

We consider several sources of systematic uncertainties that could affect our measurement of the CP violation parameters. These are calculated separately for the Belle and Belle II

datasets in MR1 and MR2. The various sources of systematics and their contributions are summarised in Tables 4 and 5 for S and C , respectively.

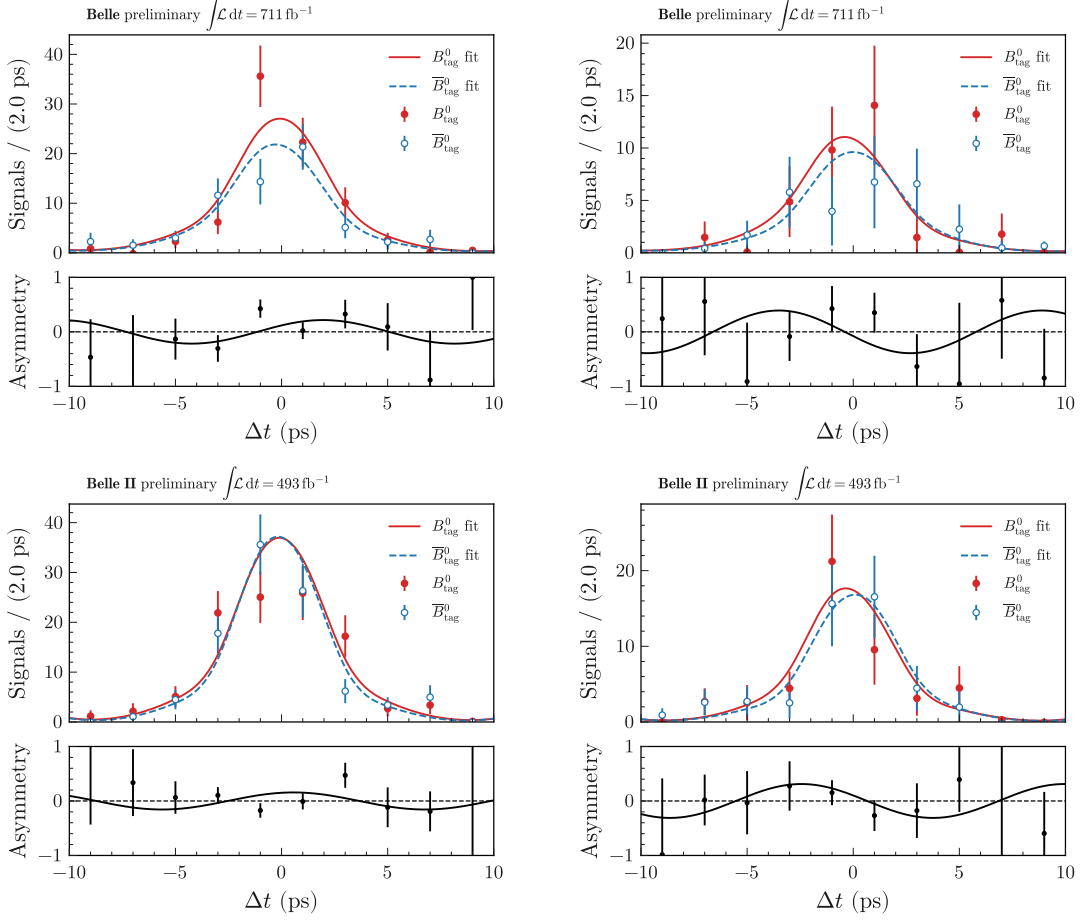


Figure 3: Fit projections for background subtracted Δt distribution for the signal component in the TD dataset for MR1 (top left), MR2 (top right) in Belle, and MR1 (bottom left), MR2 (bottom right) in Belle II. The candidates are weighted by r .

Systematic uncertainties due to the FT parameters (w , Δw , and μ), physics parameters (τ_B and Δm_d), $B\bar{B}$ CP asymmetries ($S_{B\bar{B}}$ and $C_{B\bar{B}}$), and the SCF fraction are estimated by sampling these parameters from Gaussian distributions and refitting the final dataset with these sampled values. The widths of the resulting distributions of fitted S and C values are then taken as the systematic uncertainties. For each FT parameter, the sampling Gaussian is centered at the mean value and assigned a width equal to the corresponding uncertainty, which arises from the limited size of calibration data samples. For physics parameters, the means and widths of the sampling Gaussians are set to their known values and uncertainties [28]. For $B\bar{B}$ CP asymmetries, the sampling Gaussian is centered at the values expected from MC simulation, with widths corresponding to the uncertainties in these parameters, typically around 10–20%. For the SCF fraction, the sampling Gaussian is likewise centered at its MC expected value, with a width set to 20% of that value.

The systematic uncertainties due to the fixed parameters of the resolution function and PDF shapes are estimated by sampling these parameters from the simulation-fit likelihood, and refitting the final dataset with these sampled values. The widths of the resulting distributions of fitted C and S values are taken as the systematic uncertainties. The systematic uncertainties due to non-parametric $B\bar{B}$ KDE PDFs are estimated by generating new PDFs using datasets bootstrapped from simulated events. This method introduces Poisson fluctuations on the PDF shape. The final dataset is refitted using these generated KDE PDFs and the widths of the resulting distributions of fitted C and S values are taken as the systematic uncertainties.

Systematic uncertainties related to the B meson vertex reconstruction stem from possible misalignment of vertex detectors, uncertainties in the IP profile, and corrections applied to charged track trajectories. These uncertainties are estimated using the same methodology as outlined in Refs. [10, 44]. The total vertexing systematic uncertainty is obtained by summing the individual contributions in quadrature.

Systematic uncertainties are also calculated to account for the tag-side interference effect [45]. Additionally, the fit biases on CP violation parameters obtained using randomised flavour tags are assigned as systematic uncertainties.

The uncertainties due to $B\bar{B}$ CP asymmetries, physics parameters, and tag-side interference are assumed to be 100% correlated between Belle and Belle II datasets.

Table 4: Summary of systematic uncertainties on S .

Source	Belle MR1	Belle MR2	Belle II MR1	Belle II MR2
Flavour tagging	± 0.010	± 0.019	± 0.002	± 0.004
Physics parameters	± 0.001	± 0.001	± 0.001	± 0.003
$B\bar{B}$ CP asymmetries	± 0.013	± 0.076	± 0.010	± 0.081
SCF fraction	± 0.002	± 0.006	± 0.003	± 0.005
Resolution function	± 0.018	± 0.030	± 0.007	± 0.016
PDF shape	± 0.008	± 0.024	± 0.004	± 0.030
Vertex measurement	± 0.023	± 0.024	± 0.005	± 0.015
Tag-side interference	± 0.003	± 0.004	± 0.006	± 0.001
Fit bias	± 0.005	± 0.011	± 0.001	± 0.004
Total	± 0.035	± 0.091	± 0.016	± 0.090

5 Summary

We report the measurement of time-dependent CP violation parameters in $B^0 \rightarrow K_S^0 \pi^0 \gamma$ decays using 770×10^6 and 521×10^6 $B\bar{B}$ events from Belle and Belle II, respectively. The combined values of the CP violation parameters in the $K^{*0}(892)$ region ($M_{K_S^0 \pi^0} \in [0.8, 1.0] \text{ GeV}/c^2$) are

$$S = 0.09 \pm 0.16 \pm 0.02,$$

Table 5: Summary of systematic uncertainties on C .

Source	Belle MR1	Belle MR2	Belle II MR1	Belle II MR2
Flavour tagging	± 0.021	± 0.039	± 0.007	± 0.011
Physics parameters	± 0.001	± 0.001	± 0.001	± 0.001
$B\bar{B}$ CP asymmetries	± 0.007	± 0.046	± 0.014	± 0.084
SCF fraction	± 0.001	± 0.001	± 0.002	± 0.002
Resolution function	± 0.002	± 0.006	± 0.003	± 0.005
PDF shape	± 0.003	± 0.013	± 0.007	± 0.011
Vertex measurement	± 0.006	± 0.009	± 0.002	± 0.003
Tag-side interference	± 0.036	± 0.036	± 0.034	± 0.036
Fit bias	± 0.001	± 0.005	± 0.003	± 0.002
Total	± 0.043	± 0.072	± 0.038	± 0.093

and

$$C = -0.09 \pm 0.08 \pm 0.04.$$

Similarly, the combined values of the CP violation parameters in the non- $K^{*0}(892)$ region ($M_{K_S^0\pi^0} \in (1.0, 1.8] \text{ GeV}/c^2$) are

$$S = -0.32 \pm 0.33 \pm 0.09,$$

and

$$C = -0.07 \pm 0.17 \pm 0.08.$$

These results represent the most precise measurements to date for $B^0 \rightarrow K_S^0\pi^0\gamma$, improving upon the combination of the previous Belle [11] and Belle II [13] results by approximately 24% for S and 31% for C in the $K^{*0}(892)$ region, and supersede the earlier measurements [11, 13] for the same channel. These findings are consistent with the predictions of the Standard Model.

Acknowledgements

This work, based on data collected using the Belle II detector, which was built and commissioned prior to March 2019, and data collected using the Belle detector, which was operated until June 2010, was supported by Higher Education and Science Committee of the Republic of Armenia Grant No. 23LCG-1C011; Australian Research Council and Research Grants No. DP200101792, No. DP210101900, No. DP210102831, No. DE220100462, No. LE210100098, and No. LE230100085; Austrian Federal Ministry of Education, Science and Research, Austrian Science Fund (FWF) Grants DOI: 10.55776/P34529, DOI: 10.55776/J4731, DOI: 10.55776/J4625, DOI: 10.55776/M3153, and DOI: 10.55776/PAT1836324, and Horizon 2020 ERC Starting Grant No. 947006 “InterLeptons”; Natural Sciences and Engineering Research Council of Canada, Digital Research Alliance of Canada, and Canada Foundation for Innovation; National Key R&D Program of China under Contract No. 2024YFA1610503,

and No. 2024YFA1610504 National Natural Science Foundation of China and Research Grants No. 11575017, No. 11761141009, No. 11705209, No. 11975076, No. 12135005, No. 12150004, No. 12161141008, No. 12405099, No. 12475093, and No. 12175041, and Shandong Provincial Natural Science Foundation Project ZR2022JQ02; the Czech Science Foundation Grant No. 22-18469S, Regional funds of EU/MEYS: OPJAK FORTE CZ.02.01.01/00/22_008/0004632 and Charles University Grant Agency project No. 246122; European Research Council, Seventh Framework PIEF-GA-2013-622527, Horizon 2020 ERC-Advanced Grants No. 267104 and No. 884719, Horizon 2020 ERC-Consolidator Grant No. 819127, Horizon 2020 Marie Skłodowska-Curie Grant Agreement No. 700525 “NIOBE” and No. 101026516, and Horizon Europe Marie Skłodowska-Curie Staff Exchange project JENNIFER3 Grant Agreement No. 101183137 (European grants); L’Institut National de Physique Nucléaire et de Physique des Particules (IN2P3) du CNRS under Project Identification No. CNRS-IN2P3-14-PP-033 and L’Agence Nationale de la Recherche (ANR) under Grant No. ANR-23-CE31-0018 and ANR-25-CE31-1333 (France); BMFTR, DFG, HGF, MPG, and AvH Foundation (Germany); Department of Atomic Energy under Project Identification No. RTI 4002, Department of Science and Technology, and UPES SEED funding programs No. UPES/R&D-SEED-INFRA/17052023/01 and No. UPES/R&D-SOE/20062022/06 (India); Israel Science Foundation Grant No. 2476/17, U.S.-Israel Binational Science Foundation Grant No. 2016113, and Israel Ministry of Science Grant No. 3-16543; Istituto Nazionale di Fisica Nucleare and the Research Grants BELLE2, and the ICSC – Centro Nazionale di Ricerca in High Performance Computing, Big Data and Quantum Computing, funded by European Union – NextGenerationEU; Japan Society for the Promotion of Science, Grant-in-Aid for Scientific Research Grants No. 16H03993, No. 16H06492, No. 16K05323, No. 17H01133, No. 17H05405, No. 18K03621, No. 18H03710, No. 18H05226, No. 19H00682, No. 20H05850, No. 20H05858, No. 22H00144, No. 22K14056, No. 22K21347, No. 23H05433, No. 26220706, No. 26400255, and No. 26H02056, and the Ministry of Education, Culture, Sports, Science, and Technology (MEXT) of Japan; National Research Foundation (NRF) of Korea Grants No. 2021R1-F1A-1064008, No. 2022R1-A2C-1003993, No. RS-2018-NR031074, No. RS-2021-NR060129, No. RS-2024-00354342, No. RS-2025-02219521, No. RS-2026-25471491, No. RS-2026-25480677, and No. RS-2026-25486791, Radiation Science Research Institute, Foreign Large-Size Research Facility Application Supporting project, the Global Science Experimental Data Hub Center, the Korea Institute of Science and Technology Information (K26L1M2C3) and KREONET/GLORIAD; Universiti Malaya RU grant, Akademi Sains Malaysia, and Ministry of Education Malaysia; Frontiers of Science Program Contracts No. FOINS-296, No. CB-221329, No. CB-236394, No. CB-254409, and No. CB-180023, and SEP-CINVESTAV Research Grant No. 237 (Mexico); the Polish Ministry of Science and Higher Education and the National Science Center; the Ministry of Science and Higher Education of the Russian Federation and the HSE University Basic Research Program, Moscow; University of Tabuk Research Grants No. S-0256-1438 and No. S-0280-1439 (Saudi Arabia); Slovenian Research Agency and Research Grants No. J1-50010 and No. P1-0135; Ikerbasque, Basque Foundation for Science, State Agency for Research of the Spanish Ministry of Science and Innovation through Grant No. PID2022-136510NB-C33, Spain, Agencia Estatal de Investigacion, Spain Grant No. RYC2020-029875-I and Generalitat Valenciana,

Spain Grant No. CIDEAGENT/2018/020; the Swiss National Science Foundation; The Knut and Alice Wallenberg Foundation (Sweden), Contracts No. 2021.0174, No. 2021.0299, and No. 2023.0315; National Science and Technology Council, and Ministry of Education (Taiwan); Thailand Center of Excellence in Physics; TUBITAK ULAKBIM (Turkey); National Research Foundation of Ukraine, Project No. 2020.02/0257, and Ministry of Education and Science of Ukraine; the U.S. National Science Foundation and Research Grants No. PHY-1913789 and No. PHY-2111604, and the U.S. Department of Energy and Research Awards No. DE-AC06-76RLO1830, No. DE-SC0007983, No. DE-SC0009824, No. DE-SC0009973, No. DE-SC0010007, No. DE-SC0010073, No. DE-SC0010118, No. DE-SC0010504, No. DE-SC0011784, No. DE-SC0012704, No. DE-SC0019230, No. DE-SC0021616, No. DE-SC0022350, No. DE-SC0023470; and the Vietnam Academy of Science and Technology (VAST) under Grant No. DL0000.05/26-27.

These acknowledgements are not to be interpreted as an endorsement of any statement made by any of our institutes, funding agencies, governments, or their representatives.

We thank the SuperKEKB team for delivering high-luminosity collisions; the KEK cryogenics group for the efficient operation of the detector solenoid magnet and IBelle on site; the KEK Computer Research Center for on-site computing support; the NII for SINET6 network support; and the raw-data centers hosted by BNL, DESY, GridKa, IN2P3, INFN, PNNL/EMSL, and the University of Victoria.

References

- [1] D. Atwood, M. Gronau and A. Soni, *Mixing-induced CP asymmetries in radiative B decays in and beyond the Standard Model*, *Phys. Rev. Lett.* **79** (1997) 185.
- [2] J.L. Hewett, *Probing new physics in the B system*, *AIP Conference Proceedings* **424** (1998) 328.
- [3] P. Ball, G.W. Jones and R. Zwicky, *B → Vγ beyond QCD factorization*, *Phys. Rev. D* **75** (2007) 054004.
- [4] B. Grinstein, Y. Grossman, Z. Ligeti and D. Pirjol, *Photon polarization in B → Xγ in the Standard Model*, *Phys. Rev. D* **71** (2005) 011504.
- [5] B. Grinstein and D. Pirjol, *CP asymmetry in B⁰(t) → K_s⁰π⁰γ in the Standard Model*, *Phys. Rev. D* **73** (2006) 014013.
- [6] A.L. Kagan and M. Neubert, *Direct CP violation in B → X_sγ decays as a signature of new physics*, *Phys. Rev. D* **58** (1998) 094012 [[hep-ph/9803368](#)].
- [7] F.-S. Yu, E. Kou and C.-D. Lü, *Photon polarization in the b → sγ processes in the left-right symmetric model*, *JHEP* **12** (2013) 102.
- [8] H. Eberl, K. Hidaka, E. Ginina and A. Ishikawa, *Imprint of SUSY in radiative B-meson decays*, *Phys. Rev. D* **104** (2021) 075025.
- [9] M. Jung, X.-Q. Li and A. Pich, *Exclusive radiative B-meson decays within the aligned two-Higgs-doublet model*, *JHEP* **10** (2012) 063.
- [10] BELLE II collaboration, *New graph-neural-network flavor tagger for Belle II and measurement of sin 2φ₁ in B⁰ → J/ψK_s⁰ decays*, *Phys. Rev. D* **110** (2024) 012001.

- [11] BELLE collaboration, *Time-Dependent CP Asymmetries in $B^0 \rightarrow K_s^0 \pi^0 \gamma$ transitions*, *Phys. Rev. D* **74** (2006) 111104.
- [12] BABAR collaboration, *Measurement of Time-Dependent CP Asymmetry in $B^0 \rightarrow K_s^0 \pi^0 \gamma$ Decays*, *Phys. Rev. D* **78** (2008) 071102.
- [13] BELLE II collaboration, *Measurement of CP Asymmetries in $B^0 \rightarrow K_s^0 \pi^0 \gamma$ Decays at Belle II*, *Phys. Rev. Lett.* **134** (2025) 011802.
- [14] BELLE collaboration, *The Belle detector*, *Nucl. Instrum. Meth.* **A479** (2002) 117.
- [15] S. Kurokawa and E. Kikutani, *Overview of the KEKB accelerators*, *Nucl. Instrum. Meth.* **A499** (2003) 1.
- [16] BELLE II collaboration, *Belle II Technical Design Report*, [1011.0352](#).
- [17] K. Akai, K. Furukawa and H. Koiso, *SuperKEKB collider*, *Nucl. Instrum. Meth.* **A907** (2018) 188.
- [18] BELLE II SVD collaboration, *The design, construction, operation and performance of the Belle II silicon vertex detector*, *JINST* **17** (2022) P11042.
- [19] H. Atmacan, M. Belhorn, Y. Guan, L. Li, B. Pal, S. Sandilya et al., *The imaging Time-of-Propagation detector at Belle II*, *Nucl. Instrum. Meth.* **A1080** (2025) 170627.
- [20] D.J. Lange, *The EvtGen particle decay simulation package*, *Nucl. Instrum. Meth.* **A462** (2001) 152.
- [21] S. Jadach, B.F.L. Ward and Z. Wař, *The precision Monte Carlo event generator KK for two-fermion final states in e^+e^- collisions*, *Comput. Phys. Commun.* **130** (2000) 260.
- [22] T. Sjöstrand, P. Edén, C. Friberg, L. Lönnblad, G. Miu, S. Mrenna et al., *High-energy-physics event generation with PYTHIA 6.1*, *Comput. Phys. Commun.* **135** (2001) 238.
- [23] T. Sjöstrand, S. Ask, J.R. Christiansen, R. Corke, N. Desai, P. Ilten et al., *An Introduction to PYTHIA 8.2*, *Comput. Phys. Commun.* **191** (2015) 159.
- [24] R. Brun, F. Bruyant, M. Maire, A.C. McPherson and P. Zancarini, *GEANT 3*. Geneva, 1987.
- [25] GEANT4 collaboration, *GEANT4: A simulation toolkit*, *Nucl. Instrum. Meth.* **A506** (2003) 250.
- [26] BELLE II Framework Software Group, *The Belle II Core Software*, *Comput. Softw. Big Sci.* **3** (2019) 1.
- [27] M. Gelb, T. Keck, M. Prim, C. Pulvermacher, M. Ritter, E. Hennequin et al., *B2BII: Data Conversion from Belle to Belle II*, *Comput. Softw. Big Sci.* **2** (2018) 9.
- [28] Particle Data Group, *Review of Particle Physics*, *Phys. Rev. D* **110** (2024) 030001.
- [29] BELLE collaboration, *Measurement of time-dependent CP asymmetries in $B^0 \rightarrow K_s^0 \eta \gamma$ decays*, *Phys. Rev. D* **97** (2018) 092003.
- [30] M. Feindt and U. Kerzel, *The NeuroBayes neural network package*, *Nucl. Instrum. Meth.* **A559** (2006) 190.
- [31] G. Ke, Q. Meng, T. Finley, T. Wang, W. Chen, W. Ma et al., *LightGBM: a highly efficient gradient boosting decision tree*, in *Proceedings of the 31st International Conference on Neural Information Processing Systems, NIPS'17*, (Red Hook, NY, USA), p. 3149–3157, Curran Associates Inc., 2017, <https://dl.acm.org/doi/10.5555/3294996.3295074>.

- [32] T. Chen and C. Guestrin, *XGBoost: A Scalable Tree Boosting System*, in *Proceedings of the 22nd ACM SIGKDD International Conference on Knowledge Discovery and Data Mining (KDD '16)*, pp. 785–794, ACM, 2016, DOI.
- [33] BELLE and BELLE II collaborations, *Measurement of branching fractions, CP asymmetry, and isospin asymmetry for $B \rightarrow \rho\gamma$ decays using Belle and Belle II data*, *Phys. Rev. D* **111** (2025) L071103.
- [34] BELLE II Analysis Software Group, *Global decay chain vertex fitting at Belle II*, *Nucl. Instrum. Meth.* **A976** (2020) 164269.
- [35] Eds. A. J. Bevan, B. Golob, Th. Mannel, S. Prell and B. D. Yabsley, *The Physics of the B Factories, Chapter 7.1.1*, *Eur. Phys. J.* **C74** (2014) 3026 [1406.6311].
- [36] S. Dey and A. Soffer, *Beam-Constrained Vertexing for B Physics at the Belle II Experiment*, *Springer Proc. Phys.* **248** (2020) 411.
- [37] J. Gaiser, *Charmonium spectroscopy from radiative decays of the J/ψ and ψ'* , Ph.D. thesis, Stanford University, 1982.
- [38] T. Skwarnicki, *A study of the radiative CASCADE transitions between the Upsilon-Prime and Upsilon resonances*, Ph.D. thesis, Cracow, INP, 1986.
- [39] N.L. Johnson, *Systems of frequency curves generated by methods of translation*, *Biometrika* **36** (1949) 149.
- [40] K. Cranmer, *Kernel estimation in high-energy physics*, *Comput. Phys. Commun.* **136** (2001) 198.
- [41] ARGUS collaboration, *Search for hadronic $b \rightarrow u$ decays*, *Phys. Lett. B* **241** (1990) 278.
- [42] M. Pivk and F.R. Le Diberder, *sPlot: A statistical tool to unfold data distributions*, *Nucl. Instrum. Meth.* **A555** (2005) 356 [physics/0402083].
- [43] A. Valassi, *Combining correlated measurements of several different physical quantities*, *Nucl. Instrum. Meth.* **500** (2003) 391.
- [44] BELLE collaboration, *Precise Measurement of the CP Violation Parameter $\sin 2\phi_1$ in $B^0 \rightarrow (c\bar{c})K^0$ Decays*, *Phys. Rev. Lett.* **108** (2012) 171802.
- [45] O. Long, M. Baak, R.N. Cahn and D. Kirkby, *Impact of tag-side interference on time-dependent CP asymmetry measurements using coherent $B^0\bar{B}^0$ pairs*, *Phys. Rev. D* **68** (2003) 034010.